Chemical Science

Check for updates

Sulfur-bridged chromophores for photofunctional materials: using sulfur oxidation state to tune electronic and structural properties

Jennifer Yuan, [ID] † Zhen Xu [ID] † and Michael O. Wolf [ID] *

The use of a heteroatom, such as sulfur, as a linker or bridge, in π-conjugated materials has advantages over purely carbon-based ones due to the accessibility of higher oxidation states as a result of hypervalence. Materials containing a sulfide bridge (S) can be systemically oxidized into sulfoxides (SO) and sulfones (SO$_2$), each of which can then influence how a material interacts with light, playing a large role in dictating the photophysical and sometimes photochemical properties. In this perspective, we summarize the progress that our group and others have made, showing how oxidation of a sulfur bridge in symmetric bichromophoric dimers and in diimine ligands can influence the excited state behavior in organic π-conjugated materials and metal complexes.

Introduction

Sulfur is an essential element for all living organisms and is utilized biologically in various oxidation states. The oxidation and reduction of sulfur and its compounds occurs in different species of bacteria and plants.[1,2] *Chromatia* oxidize sulfides *via* elemental sulfur to sulfate, whereas sulfur assimilation (reduction of sulfates into sulfides by plants) is a vital metabolic pathway to form the amino acids cysteine and methionine.[3] Furthermore, sulfhydryl groups of cysteine residues found in proteins can be oxidized to disulfide bridges, playing an important role in the stability of proteins by maintaining tertiary structures.[4,5] The various biological functions of sulfur

are related to its hypervalence, which allows for oxidation–reduction transformations to occur. Due to the accessibility and reactivity of sulfur in different oxidation states, sulfur-containing molecules are now widely used in the fields of pharmaceuticals,[6] agrochemicals,[7,8] and materials.[9] Contributions to such diverse fields highlight the importance of design and synthesis of novel organosulfur compounds.[3]

Sulfur-containing heterocycles have been extensively used in organic semiconductors for electronic applications in organic light-emitting devices (OLEDs)[10–12] and organic field-effect transistors (OFETs).[12–16] Among these, thiophene-based systems are one of the most versatile conjugated materials due to their stability and ease of synthetic modification resulting in controllable optical properties, good charge mobility and low band gaps.[11,17,18] As such, methods to increase the fluorescence efficiency and modulate the redox properties of thiophene building blocks have been widely explored to enhance

Department of Chemistry, University of British Columbia, 2036 Main Mall, Vancouver, British Columbia, V6T 1Z1, Canada. E-mail: mwolf@chem.ubc.ca

† J. Y. and Z. X. contributed equally to this work.

Jennifer Yuan received her BSc in Chemistry at Western University and her PhD at the University of British Columbia with Michael Wolf. Her research was focused on designing new sulfur-bridged chromophore dimers and studying their resulting photophysical and photochemical properties. She is currently a Postdoctoral Associate with Aaron Beeler at Boston University.

Zhen Xu received his BSc in Chemistry at Wuhan University and his PhD at the University of British Columbia with Michael Wolf. His research was focused on designing new inorganic and organic photochromic and luminescent materials. He is currently a Mitacs Postdoctoral Fellow with Mark MacLachlan at the University of British Columbia.

the performance of such devices. Oxidation of the thienyl sulfur to S,S-dioxides was a strategy first proposed by Tanaka to lower the HOMO–LUMO gap in oligothiophenes.[19] Barbarella was the first to synthesize a series of oligothiophenes with S,S-dioxide moieties and demonstrate effectiveness of this strategy in enhancing luminescence efficiency, in particular in the solid-state.[20–22] Since then, numerous studies on the effect of oxidation on oligothiophenes have been carried out.[23–25] While oxidation of heterocyclic sulfur atoms has shown promising results, the incorporation of a sulfur atom as a linker group or bridge provides an interesting design principle for conjugated materials. Electronic interactions between conjugated rings mediated by sulfur bridges may be possible and could result in interesting new electronic properties. Additionally, higher oxidation states are intriguing, and are not available for carbon-based (saturated and unsaturated) linkers where hypervalence is not possible.

To develop efficient solar cells, researchers have taken inspiration from nature, mimicking light harvesting (LH) complexes used in photosynthesis. LH complexes contain an antenna composed of an assembly of hierarchically ordered identical chromophores, which deliver energy (from absorbed photons) efficiently over a large distance, to the reaction center where electron and hole separation occurs. A clear understanding of the excited state properties and their organization is required in fabricating artificial systems. The magnitude of electronic coupling (degree of electronic interactions between neighboring molecules) plays an important role in dictating the rate of the electron and energy transfer processes that occur in these large assemblies.[26,27] Efficient coupling can be induced in crystals,[28] aggregates[29,30] and covalent dimers[31,32] via through-space or through-bond interactions. In covalently linked systems, rates of energy and electron transfer can be precisely controlled. Through rational design, the linker (or bridge) can bring together the subunits in the correct orientation and distance, inducing characteristic properties compared to the corresponding monomers due to their closely packed π-

systems. Additionally, the bridge can participate electronically through through-bond interactions.

In this perspective, we highlight two classes of sulfur-bridged bichromophoric dimers found in (1) organic π-conjugated materials and as (2) ligands for luminescent transition metal complexes (Fig. 1). In addition, we focus on the unique photophysical and photochemical phenomena that arise from different oxidation states. Herein, we review the most recent progress made by our group and others.

Role of sulfur bridges in bichromophoric systems

Sulfur has been previously used as a non-conjugated bridge to covalently link identical chromophores to induce interchromophoric interactions. Depending on the position and type (sulfide versus disulfide) of linker, the degree of electronic coupling can be controlled by the orientation of the π-systems. For example, the photophysical properties resulting from the dimerization of boron difluoride (BF_2) complexes using such bridges have been examined by several groups. In these cases, the dimers were often compared to their monomeric species (a single chromophore with a sulfur substituent) and the effect of oxidation on electronic coupling was not examined.
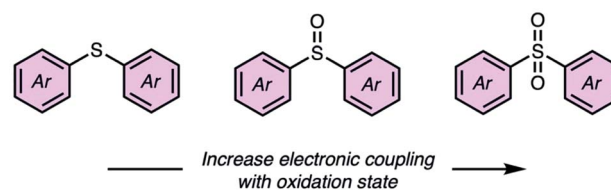
Bröring bridged boron dipyrromethenes (BODIPYs) using sulfur to form dimers 1a–1c (Fig. 2a).[29] Regioisomers 1a and 1c (α- versus β-linked, respectively) with sulfur bridges were used to study the effect of the linking position, and the distance between the subunits was varied by increasing the number of sulfur atoms in the bridge using compound 1b (sulfide versus disulfide). Both sulfide- and disulfide-bridged dimers 1a and 1b exhibit exciton coupling with splitting of the S_1 level, observed as two peaks in the absorption spectrum (Fig. 2b). This splitting is more pronounced for sulfide 1a than disulfide 1b, due to the closer spatial arrangement of the BODIPY subunits. β-Sulfur-bridged dimer 1c exhibits less exciton splitting than 1a and 1b, which the authors attribute to increased distance between

Michael Wolf received his BSc in Biochemistry and Chemistry at Dalhousie University and his PhD at the Massachusetts Institute of Technology with Mark Wrighton. He then completed a one-and-a-half-year stint as a NSERC Post-doctoral Fellow at the University of Texas-Austin with Marye Anne Fox. He has been on the faculty at the University of British Columbia since 1995 and is now a full Professor and Head of the Department. He was elected a Fellow of the Chemical Institute of Canada in 2015 and his major contributions are to the fields of conjugated polymers and materials, the photochemistry and photophysics of conjugated materials and coordination complexes, and the synthesis of and applications of modified nanomaterials.
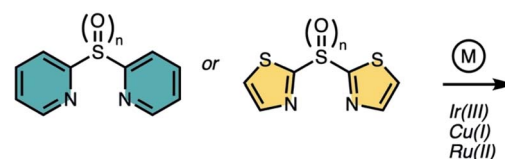

Fig. 1 Introduction of sulfur bridges into (1) organic π-conjugated materials and (2) ligands, as a molecular design strategy for controlling electronic coupling and photophysical properties of luminescent transition metal complexes as a function of oxidation state ($n = 0–2$).
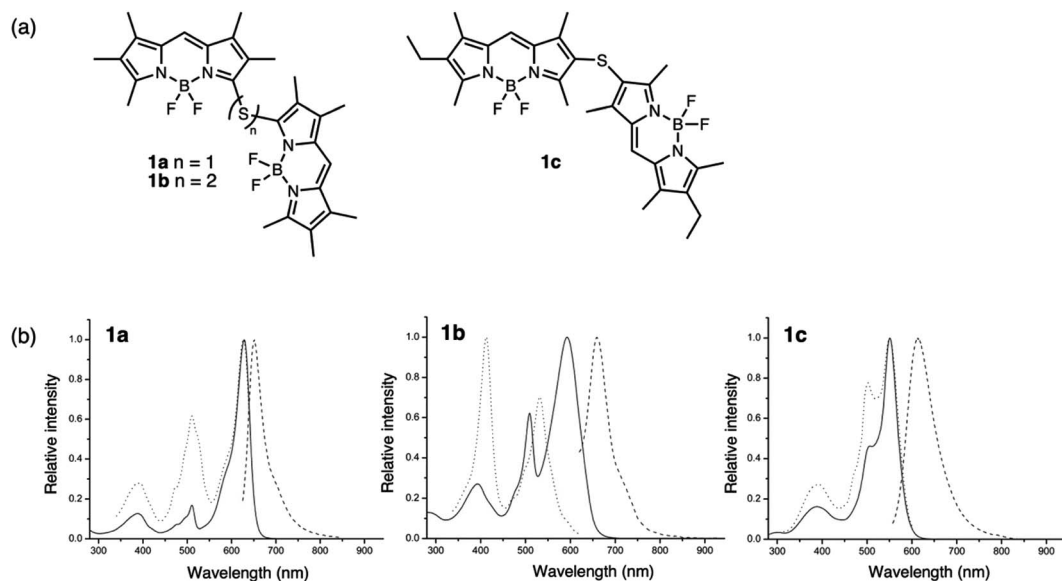
Fig. 2 (a) Structures of α- or β-sulfide-bridged **1a** and **1c** and α-disulfide-bridged **1b** BODIPY dimers reported by Bröring. (b) UV-vis absorption (solid line), emission (dashed line) and excitation (dotted line) spectra of the dimers in CH_2Cl_2. Adapted with permission from ref. 29. Copyright 2013 Wiley.

the subunits linked through the β-position compared to the α-position. Both sulfides **1a** and **1c** exhibit negative solvatochromic behavior in emission, with enhanced quantum yields in nonpolar solvents, suggesting an intramolecular charge transfer (ICT) process in the excited state under solvent-induced symmetry breaking. In contrast, the excited state behavior of disulfide **1b** is not influenced by solvent polarity and intramolecular excimer formation is proposed for low quantum yields. Here, the position and length of the sulfur bridge is used to control the relative orientation of the BODIPY subunits which influences the intensity of exciton splitting.

Boron complexes linked together in the *meso*-position should show greater overlap of their π-systems than α- or β-linked dimers due to the increased dihedral angle θ which can influence the electronic properties (Fig. 3b). Maeda used a disulfide bridge to bridge two boron dipyrrolyldiketones in the *meso*-position to form dimers **2a** and **2b** (Fig. 3a).[33] Although disulfide bonds show typical θ of 90° to 100°, smaller θ for more efficient π-overlap can be achieved using intramolecular bonding interactions between the subunits. A blue-shift with the appearance of a shoulder band in the absorption spectrum of dimer **2a** (Fig. 3c) compared to its monomer **2c** suggests the formation of "oblique H-aggregated" dimers, with dihedral angles of *ca.* 30° to 40° in solution, promoted by intramolecular π–π and N–H···F hydrogen-bonding interactions. A C–S–S–C dihedral angle of 39.4° was also estimated at the B3LYP-GD3BJ/6-31G(d,p) level of theory, in the optimized geometry, consistent with the observed absorption spectrum. Single crystal X-ray analysis of **2a** reveals a dihedral angle of 90.3°, contrasting with the results of DFT calculations. However, two pseudopolymorphs were obtained of **2b**: plates and needles, exhibiting dihedral angles of 86.7° and 39.1°, respectively. While both **2a** and **2b** (plate polymorph) showed typical C–S–S–C dihedral angles in the 90° to 100° regime, **2b** (needle polymorph) corroborates theoretical studies. In this case, the arrangement of the boron dipyrrolyldiketones subunits was held using a disulfide-bridge in the *meso*-position and with the help of intramolecular interactions, unusually small C–S–S–C angles were observed.

Sulfur-bridged porphyrins have been synthesized by Senge,[34] but their photophysical properties were not examined in detail. Related to the aforementioned BF_2 complexes are subporphyrins, a ring-contracted derivative of porphyrins developed by Kim and Osuka.[35] Subporphyrin dimers linked by sulfide and disulfide bridges through the *meso*-position (**3a** and **3b**, respectively) were synthesized and their photophysical properties were examined in detail (Fig. 4a). Sulfide **3a** exhibits exciton coupling between the two subunits observed as a split Soret-like band and broad Q-bands in the absorption spectra (Fig. 4b). The red-shifted emission profile of **3a** with a large Stokes shift (2670 cm^{-1}) indicates a substantial structural change in the excited state. Comparatively, disulfide **3b** does not exhibit exciton splitting and is non emissive (quantum yield of <0.01), suggesting that electronic perturbation by the individual subunits on each other is less than in **3a**. Likewise, contrasting transient absorption (TA) profiles were observed for sulfide **3a** *versus* disulfide **3b**. The evolution and red-shift of the transient stimulated emission (SE) band in the TA spectrum of **3a** (Fig. 4c) suggests effective electronic communication through the sulfur bridge whereas the TA spectrum of **3b** (Fig. 4d) shows a rapid decay of the singlet induced absorption, quenching the excited state. The authors suggest a deactivation pathway involving rotation along the S–S axis, originally postulated by Bröring in regard to disulfide-bridged BODIPY dimer **1b**.[29]

It has been demonstrated that incorporation of sulfide and disulfide bridges into dimeric systems can impose drastic changes to the electronic properties of the resulting materials.

Fig. 3 (a) Structures of *meso*-disulfide-bridged boron dipyrroyldiketone dimers **2a** and **2b** and monomers **2c** and **2d** reported by Maeda. (b) Cartoon representation showing how *meso*-linked chromophores have greater areas of overlap compared to α- or β-linked dimers. (c) UV-vis absorption spectra of dimer **2a** (blue) compared to monomer **2c** (red) in CH$_2$Cl$_2$. Adapted with permission from ref. 33. Copyright 2017 American Chemical Society.

The sulfide bridge can bring the subunits closer together spatially, allowing for strong electronic coupling. While disulfide bridges tend to be more flexible, separating the subunits at greater distance, intramolecular interactions within the dimer can help promote efficient electronic coupling. Additionally, depending on the position of the linkage and thus the conformation of the subunits, the strength of exciton coupling can be controlled. The bridge serves as a non-conjugated linker to enable through-space interactions between the subunits, however the question of whether the sulfur bridge participates in the electronic states was not examined in these works.

Sulfone bridges in luminescent materials

The use of a sulfone (SO$_2$) moiety as the linker has been extensively explored as an acceptor group in the design of
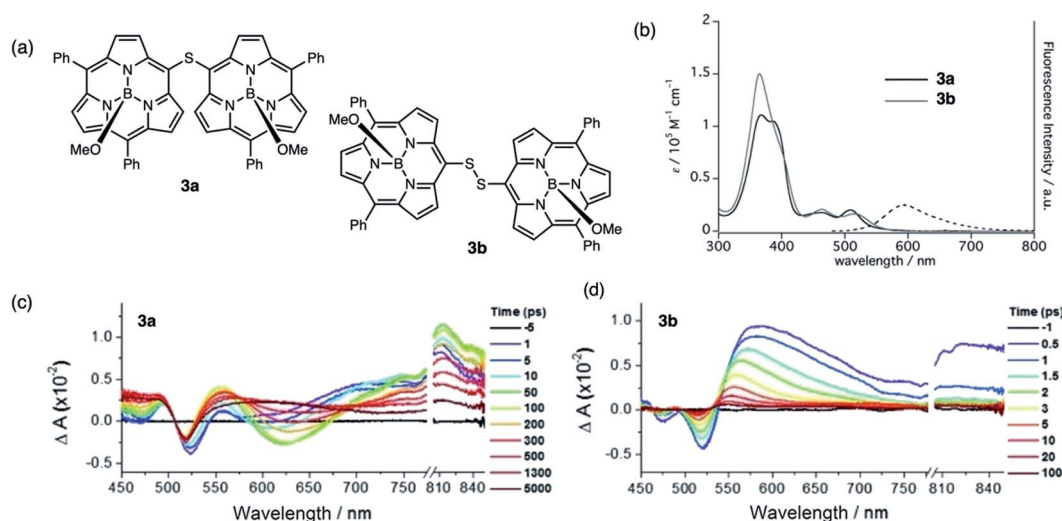

Fig. 4 (a) Structures of sulfide-bridged **3a** and disulfide-bridged **3b** subporphyrin dimers reported by Kim and Osuka. (b) UV-vis absorption (solid) and fluorescence (dashed) spectra of **3a** (black) and **3b** (gray) in CH$_2$Cl$_2$. (c and d) Transient absorption spectra of **3a** and **3b** in toluene ($\lambda_{exc} = 490$ nm). Adapted with permission from ref. 35. Copyright 2016 Wiley.

luminescent materials exhibiting thermally activated delayed fluorescence (TADF).[10,36] TADF is a radiative process from the first singlet excited state (S_1). It requires a small singlet-triplet energy gap (ΔE_{ST}) to enable reverse intersystem crossing (RISC) from the triplet excited state to the singlet excited state. This approach efficiently harvests triplet excitons through RISC and is beneficial for applications in OLEDs. The tetrahedral geometry of sulfur provides the opportunity to limit the conjugation between donors and acceptors.[37] In 2012, Adachi and co-workers prepared three compounds (**4a–4c**) with donor–acceptor-donor (D–A–D) structures.[38] The diphenyl sulfonyl acceptor in the presence of N-containing donors leads to charge transfer (CT) character in the singlet excited state, resulting in a small ΔE_{ST}. The introduction of the *tert*-butyl group enhances the donor strength while the carbazole group raises the energy level of the first triplet excited state (T_1). Therefore, **4c** shows the smallest ΔE_{ST} and highest luminescence efficiency (0.80 at 423 nm) as a film doped into a bis[2-diphenylphosphino)phenyl] ether oxide (DPEPO) host. An OLED device was also fabricated with **4c** as the emitting layer with an external quantum efficiency (EQE) of 9.9%. Replacing the *tert*-butyl group with methoxy substituents (**4d**) reduces ΔE_{ST} from 0.32 eV (**4c**) to 0.21 eV,[39] and the maximum EQE was improved to 14.5% with an emission peak at 460 nm. Since then, various donor groups (Fig. 5) have been chosen to tune ΔE_{ST} and TADF efficiency,[40–42] and features such as aggregation-induced emission (AIE) have also been imbued within the structure (**4g** and **4j**) to improve efficiency in undoped OLED devices.[41,43] In these cases, the sulfone bridge functions as the acceptor and the interaction between monomers (donor groups) was not explored.

Luminescence enhancement by sulfur oxidation

Although sulfide- and sulfone-bridged systems have been used in novel photofunctional π-conjugated materials, systematic studies on how oxidation of the sulfur bridge alters the structural and electronic properties of these materials are scarce.

Rodembusch and Silveira designed a class of asymmetric **5aSO$_n$–5bSO$_n$** and symmetric **5cSO$_n$–5eSO$_n$** dyes containing a (di)vinylsulfide bridge, which could readily be oxidized to the sulfoxide and sulfone (Fig. 6).[44,45] Oxidation increases the electron-withdrawing capacity of the sulfone as an acceptor compared to the sulfide, inducing ICT. No apparent trend in photoluminescence quantum yields (PLQYs) was noted.

In 2013, our group reported how oxidation effects the photophysical properties of symmetric sulfur-bridged chromophore dimers. The chromophores studied were bithiophene (**T$_2$**), terthiophene (**T$_3$**), naphthalene (**Nap**) and pyrene (**Pyr**) (Fig. 7a).[46] All four systems exhibited a systematic increase in their PLQYs upon oxidation of the sulfur (S) to the sulfoxide (SO) and sulfone (SO$_2$) derivatives (Fig. 7). In most cases, the sulfoxide- and sulfone-bridged dimers are more emissive than the parent arenes (Fig. 7c). It was also found that CT character, indicated by solvatochromism in the fluorescence of the compounds, is more prevalent in the sulfoxide- and sulfone-bridged species. This approach provided a general and facile method to improve
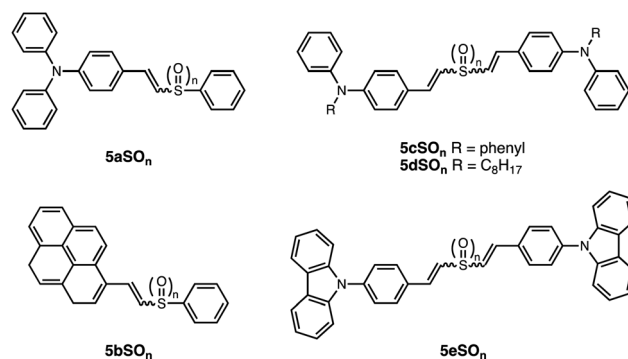

Fig. 6 Structures of asymmetric **5aSO$_n$** and **5bSO$_n$** and symmetric **5cSO$_n$** to **5eSO$_n$** dyes containing a (di)vinylsulfide bridge ($n = 0$–2) reported by Rodembusch and Silveira.
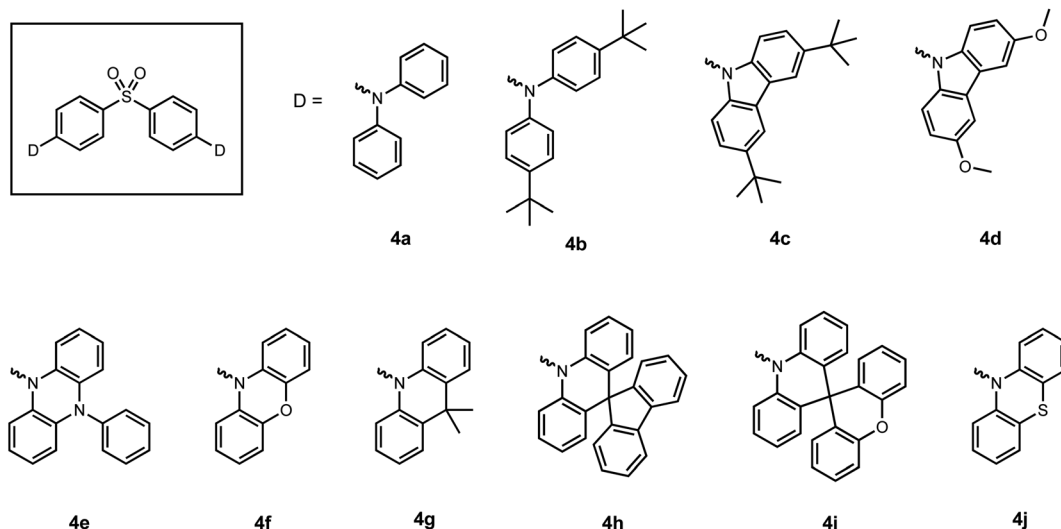

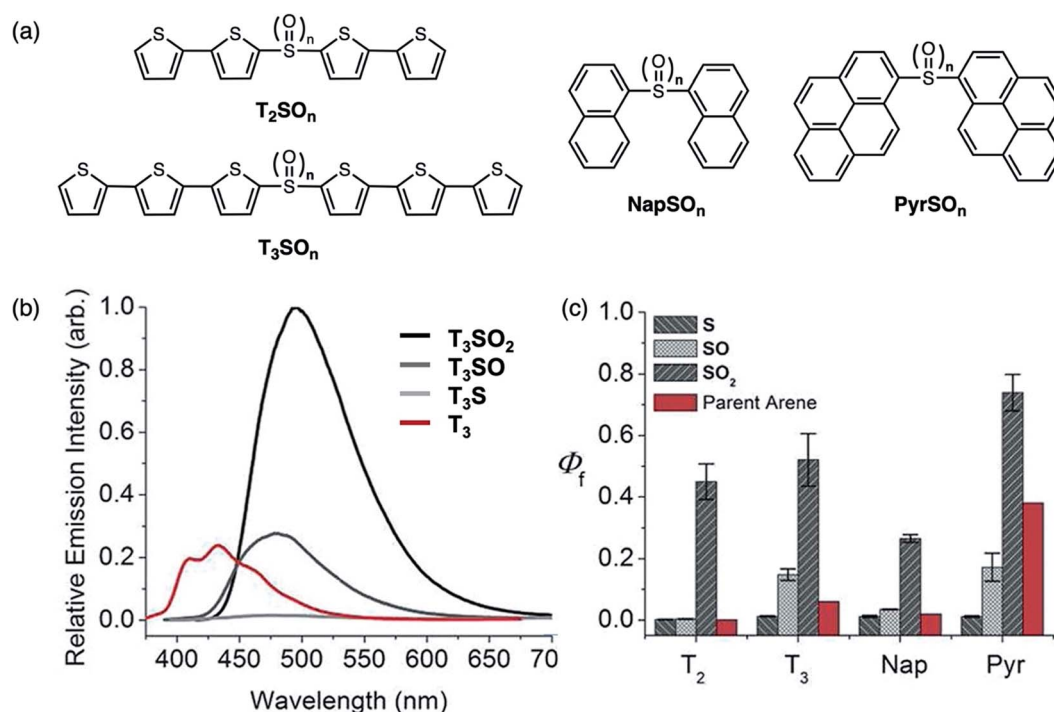Fig. 5 Structures of TADF emitters containing diphenyl sulfonyl acceptors reported previously.

Fig. 7 (a) Structures of sulfur-bridged bithiophene T_2SO_n, terthiophene T_3SO_n, naphthalene $NapSO_n$ and pyrene $PyrSO_n$ dimers ($n = 0-2$) reported by our group. (b) Emission spectra of T_3SO_n and T_3 in CH_2Cl_2. (c) Photoluminescence quantum yields (Φ_f) of sulfur-bridged dimers with increasing oxidation states, in comparison to parent arenes. Adapted with permission from ref. 45. Copyright 2013 American Chemical Society.

PLQYs in organic chromophores, which is anticipated to be beneficial for OLED applications.

The mechanism of this photoluminescence enhancement in the terthiophene dimers T_3SO_n was further investigated using ultrafast TA spectroscopy and computational approaches.[47] Methyl-terminated monomers T_3SO_nMe were synthesized as model compounds (Fig. 8a). Their fluorescence spectra are relatively invariant with increasing solvent polarity and excited state dynamics such as photoluminescence decays resemble those of parent arene T_3. These results demonstrate that the CT character originates from the interaction between two T_3 monomers and not from the linker itself. On the other hand, fast relaxation ($\sim$5 ps) from the first excited singlet state (S_1) to an intermediate singlet excited state (S_1^*) was exclusively observed in T_3SO_n dimers by femtosecond TA. This excited state exhibits solvent sensitivity and CT character. With the aid of DFT calculations, S_1^* was identified as a symmetry breaking CT state with a net dipole, in which one of the T_3 moieties

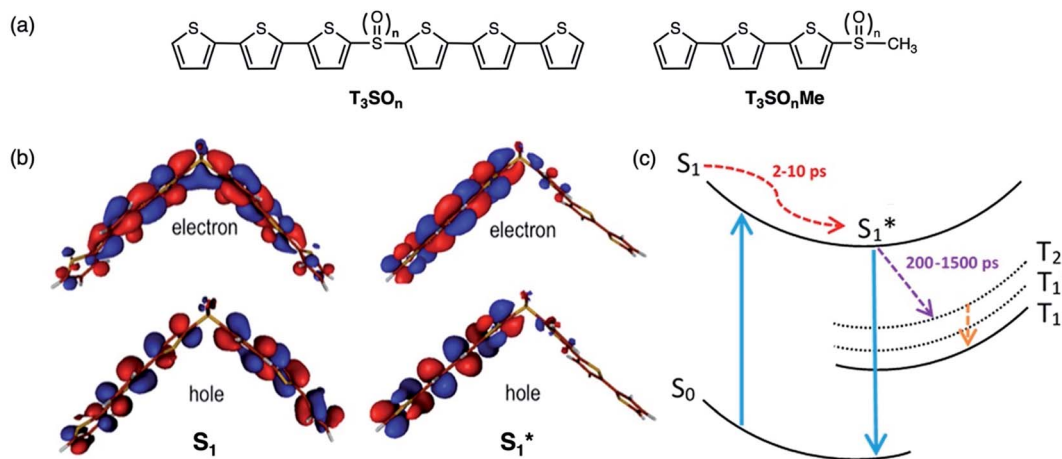**Fig. 8** (a) Structures of sulfur-bridged terthiophene dimers T_3SO_n and monomers T_3SO_nMe ($n = 0-2$) reported by our group. (b) Electron and hole natural transition orbitals (NTOs) of T_3SO_n singlet excited states S_1 and S_1^* in CH_2Cl_2. (c) Simplified Jablonski diagram illustrating the excited-state relaxation in T_3SO_n. Adapted with permission from ref. 46. Copyright 2015 American Chemical Society.
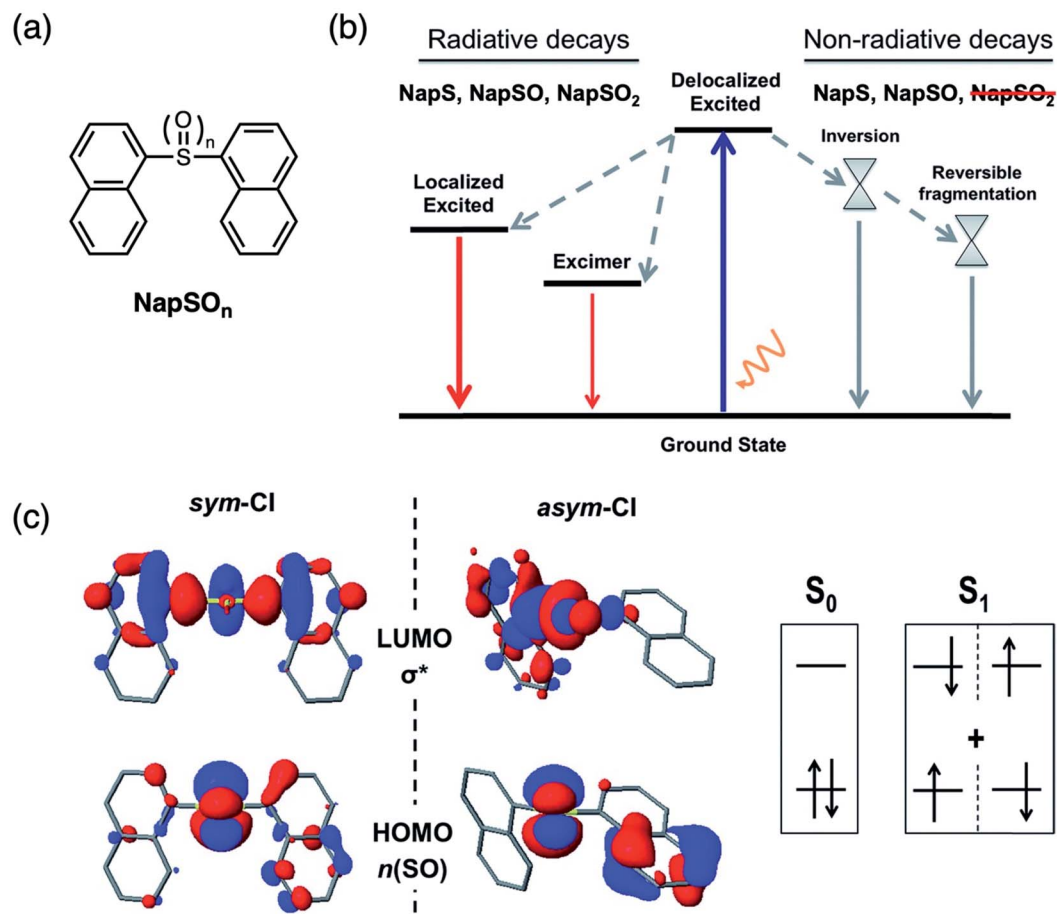
Fig. 9 (a) Structures of sulfur-bridged naphthalene dimers **NapSO**$_n$ ($n = 0-2$) reported by our group. (b) Simplified Jablonski diagram illustrating the deactivation mechanisms in **NapSO**$_n$. (c) Frontier molecular orbitals (n(SO) and σ^*) at the symmetric and asymmetric S_0/S_1 conical intersection (CI) points for **NapSO**. Adapted with permission from ref. 47. Copyright 2017 Royal Society of Chemistry.

planarizes, localizing the charge (Fig. 8b). S_1^* cannot couple efficiently with the triplet excited states due to the one electron nature of the spin–orbit operator. This leads to a decrease in ISC rate resulting in greater fluorescence efficiency compared to T_3 (Fig. 8c). Computational studies reveal that the electron lone pairs on the sulfur atom plays a role in mediating intra-molecular interactions. Specifically, they "shield" the electronic coupling between monomers by electrostatic screening and suppress relaxation to S_1^*. By oxidizing the sulfur atom, lone pair screening is reduced, and the CT state can be stabilized, which leads to the enhanced PLQYs. Not only do these findings provide insight into the excited state dynamics of sulfur-bridged dimers, but they also open the door to design of efficient organic chromophores for OLEDs and solar energy conversion.

Unlike terthiophene, naphthalene does not suffer from ISC as the major non-radiative pathway due to its planarity and lack of thienyl rings. In order to further understand the origin of enhanced emission by sulfur oxidation and to validate the lone-pair screening theory proposed above, naphthalene dimers **NapSO**$_n$ (Fig. 9a) were investigated with computational simulations.[48] In this case, the differences in PLQY were shown to be the result of energetically favorable non-radiative decay pathways available in **NapS** and **NapSO**, and not **NapSO**$_2$ (Fig. 9b),

indicating that the electron lone pairs on the sulfur atom are largely involved in such transitions. It has previously been proposed that pyramidal inversion of the excited state in aryl sulfoxides results in efficient internal conversion (IC) as the main non-radiative relaxation pathway.[49] Calculations show that this inversion is thermally accessible for the **NapSO** system, but due to a large S_0/S_1 energy gap of the inversion TS in **NapS** and **NapSO**, non-radiative relaxation by IC was ruled out as the main deactivation pathway. We identified a conical intersection (CI) (a S_0/S_1 state crossing), which is energetically accessible upon photoexcitation, allowing for relaxation back down to the ground state without emission (Fig. 9c). The lack of electron lone pairs on the sulfur in **NapSO**$_2$ blocks low-lying S_0/S_1 state crossings, resulting in much higher PLQYs compared to **NapS** and **NapSO**. Therefore, it can be concluded that the sulfur electron lone pairs dictate the excited state dynamics in sulfide and sulfoxide dimers, and sulfur oxidation is a general and novel approach for the design of strongly luminescent materials.

After demonstrating the mechanism of fluorescence enhancement by sulfur oxidation in small molecules, we further employed this strategy on oligomeric and polymeric substrates (Fig. 10a).[50] Other examples of polymeric materials which
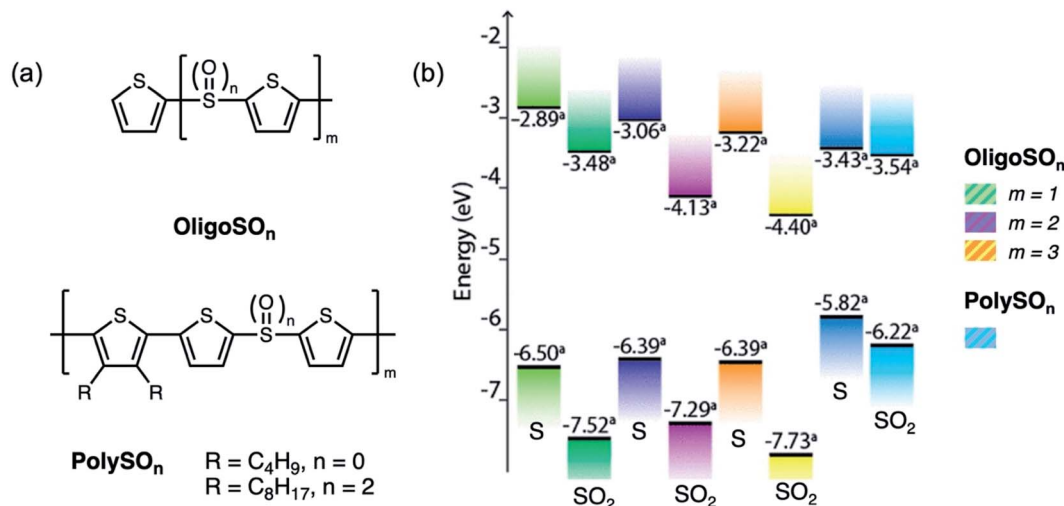
Fig. 10 (a) Structures of thiophene-based oligomers **OligoSO**$_n$ and polymers **PolySO**$_n$ containing a sulfur bridge ($n = 0, 2$) reported by our group. (b) Calculated frontier energy levels obtained from cyclic voltammetry measurements and UV-vis absorption spectra. Adapted with permission from ref. 49. Copyright 2017 American Chemical Society.

exhibit enhanced emission focus on the oxidation of thienyl sulfur in polythiophene systems.[51–54] We designed thiophene-containing oligomers and polymers in which the main backbone contained alternating (ter)thiophene and sulfide or sulfone moieties. Similar to the trend observed in the small molecules **T$_3$SO**$_n$, **OligoSO$_2$** and **PolySO$_2$** exhibited higher PLQYs than **OligoS** and **PolyS**. As the number of repeat units increases, the HOMO–LUMO gap gets smaller, and this effect is more prevalent in the sulfide-bridged system compared to the sulfone-bridged system (Fig. 10b). This suggests that the sulfone bridge insulates the interactions between the individual thienyl units. Additionally, while the energy of the HOMO–LUMO gap is lowered upon sulfur oxidation due to the electron withdrawing nature of the sulfone group, the magnitude of the energy gap is also increased upon oxidation.

Recently, organic room temperature phosphorescence (RTP) has attracted much attention due to the ability to utilize long-lived (>ms) radiative triplet states, yielding potential applications in OLEDs, data encryption, and chemical and biological sensing and imaging.[55–57] In order to increase phosphorescence efficiency, functional groups with lone pairs such as carbonyl and sulfone groups are commonly used, due to the capability of facilitating (n, π*) transitions from the first singlet excited (S$_1$) to triplet excited states (T$_n$) to enhance ISC, according to El Sayed's rule.[58,59] On the other hand, RTP lifetimes can be prolonged by utilizing the (π, π*) transition from the first triplet excited state (T$_1$) to the ground state (S$_0$).[58,59] These excited state transitions can be controlled by both molecular structure and packing. Having demonstrated that sulfide bridges can enhance intersystem crossing by lone pair screening, we examined the effects of sulfur oxidation state on RTP.[60] In the sulfur-bridged carbazole dimers **CBZSO**$_n$ (Fig. 11a), it was found that the single crystal packing modes are almost identical among three compounds with different oxidation states, providing a rare molecular model to study the electronic effects alone without

simultaneously altering the intermolecular interactions. All three compounds also exhibit similar RTP lifetimes, largely due to the strong (π, π*) character localized at carbazole groups. Unlike in **T$_3$S**, sulfur lone pairs in this case can participate in (n, π*) transitions due to the similar energy levels with the HOMO (Fig. 11c). Even though **CBZSO** has the strongest (n, π*) character indicated by its spin–orbit coupling (SOC) constant, **CBZS** shows the highest phosphorescence efficiency (Fig. 11b). It can be rationalized that the combination of the (n, π*) transition and electrostatic screening results in the sulfide having the highest phosphorescence. It is also worth noting that the oxygen lone pair orbitals in SO$_2$ lie at much lower energies and do not contribute to SOC between low-lying triplet excited states and the ground state. Sulfone groups have been extensively explored in TADF and RTP materials[38,41,61–64] while sulfides have been largely neglected. These findings provide a new perspective for the design of triplet-harvesting luminescent materials.

Oxidation-dependent photochemistry

In the search for additional chromophores to examine the effect of oxidation of the bridging sulfur on the photophysical properties, we found that when the substituent was anthracene, sulfur-bridged dimers **AnSO**$_n$ exhibited different photophysical trends than the aforementioned dimers.[65] Although anthracene belongs to the same class of molecules (polycyclic aromatic hydrocarbons) as naphthalene and pyrene, **AnSO** and **AnSO$_2$** are less emissive than **AnS**, contrasting with the behavior previously observed in **T$_2$SO**$_n$, **T$_3$SO**$_n$, **NapSO**$_n$ and **PyrSO**$_n$. The most intriguing aspect is that depending on the oxidation state, **AnSO**$_n$ undergoes different photochemical pathways.

The photochemical products of **AnSO**$_n$ are shown in Fig. 12a. Irradiation of **AnS** with UV light (365 nm) results in no photochemical reaction. Under the same conditions, irradiation of **AnSO** results in the of loss the sulfoxide bridge, producing 9,9′-bianthracene (**BA**). The photochemical reaction of **AnSO** to **BA**

Fig. 11 (a) Structures of sulfur-bridged carbazole dimers **CBZSO$_n$** reported by our group. (b) Time-resolved photoluminescence spectra (60 μs to 110 ms time range) of **CBZS**, **CBZSO** and **CBZSO$_2$** crystalline samples under ambient conditions at 298 K. The intensity is corrected by fluorescence integration under the same excitation condition as time-resolved measurements and PLQYs. (c) Schematic comparison of frontier orbitals in terthiophene (**T$_3$S**) and carbazole (**CBZS**) sulfur-bridged dimers. Adapted with permission from ref. 59. Copyright 2021 Royal Society of Chemistry.

can be monitored using absorption and emission spectroscopies (Fig. 12b and c). Upon conversion to **BA**, there is a significant increase in the PL intensity. Kinetic studies indicate that the formation of **BA** is sensitive to the presence of oxygen, and along with triplet sensitization studies using [Ru(bpy)$_3$]$^{2+}$, suggests the involvement of a triplet excited state. It is not yet known whether sulfur monoxide (SO) is generated from this photolysis reaction. Other examples of sulfur monoxide release from sulfoxides by photolysis have been observed in *peri*-substituted trisulfide-2-oxides reported by Grainger[66] and in dinaphthothiepine bisimide sulfoxide reported by Fukui and Shiokubo.[67] On the other hand, the generation of sulfur monoxide by thermal methods has been studied using episulfoxides since the 1960s.[68–71] In recent years, both organic and main group precursors[72,73] capable of sulfoxide extrusion reactions have been developed.

Irradiation of **AnSO$_2$** yields a dimer containing a three-membered episulfone ring **AnD**, which can thermally revert to the starting bridged species in the dark. The formation of anthracene dimers by [4 + 4] photodimerization (intermolecular) or photocycloisomerization (intramolecular) reactions has been known since 1867 and has been extensively studied and reviewed.[74,75] With prolonged irradiation times (overnight) in the presence of oxygen, **AnSO$_2$** forms anthraquinone **Anq**.

We sought to investigate why **AnS** (unoxidized) is unreactive, whereas **AnSO$_2$** (fully oxidized) undergoes a photochemical reaction.[76] Phenyl-terminated monomers **AnSO$_n$Ph** were synthesized as model compounds (Fig. 13a). The solvent-dependent PL lifetimes with a monoexponential decay profile of **AnS** and **AnSPh** (Fig. 13b) suggests an excited state with CT character, which undergoes rapid non-radiative relaxation, faster than monomeric anthracene **An**. TA studies identify a population transfer between the singlet and triplet excited states, indicative of ISC. Since the singlet state has appreciable CT character, the energy of the singlet is lowered in solvents of increasing polarity, which brings this state closer in energy to the triplet, facilitating rapid ISC. In the sulfone-bridged systems, phenyl-terminated **AnSO$_2$Ph** also exhibits solvent-dependent monoexponential PL decay similar to **AnS** and **AnSPh**. In this case, there is no observation of a triplet feature in the TA spectrum, suggesting IC and not ISC, as the main non-radiative deactivation pathway, quenching PL. However, **AnSO$_2$** exhibits biexponential PL decays in all solvents (Fig. 13c). The TA data suggests that a portion of the singlet population in
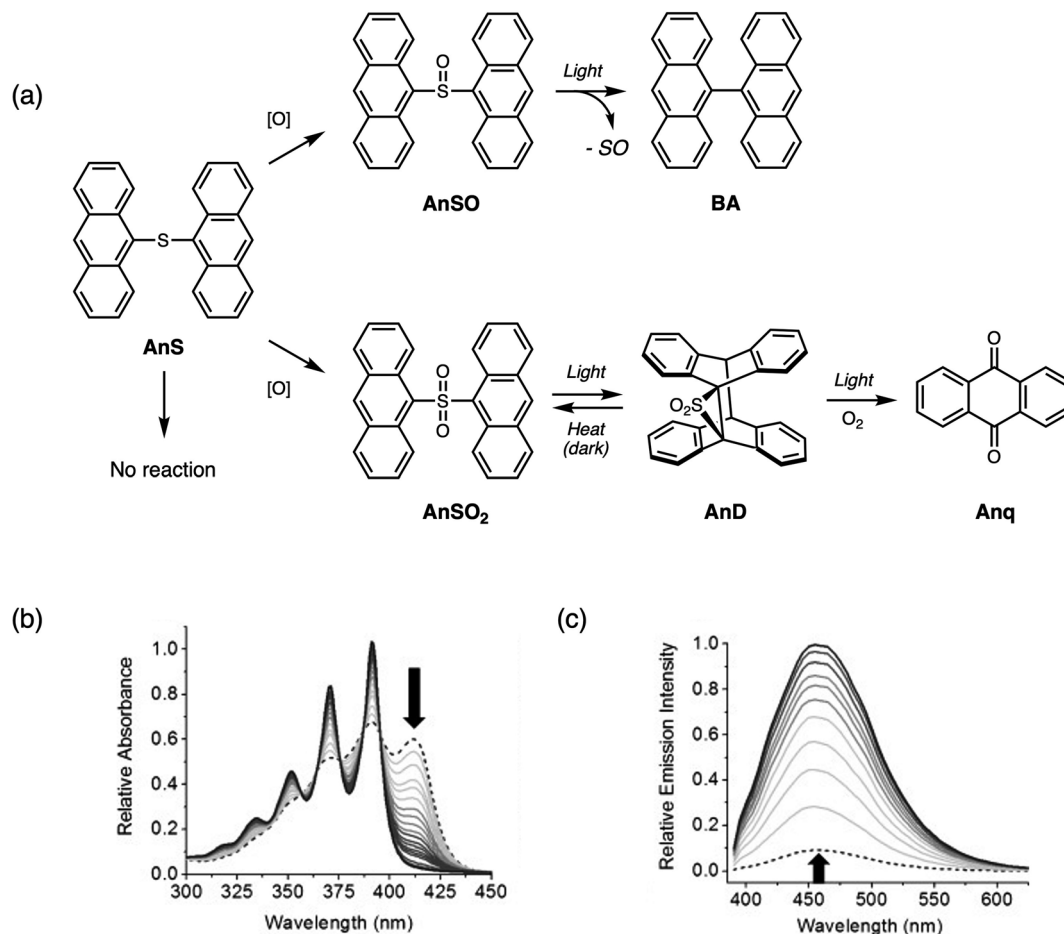
Fig. 12 (a) Different photochemical pathways of sulfur-bridged anthracene dimers AnSO$_n$ ($n = 0–2$) depending on the oxidation state. Changes in the (b) UV-vis absorption and (c) emission spectra when AnSO is irradiated with UV light in CH$_2$Cl$_2$. Adapted with permission from ref. 64. Copyright 2013 Wiley.

AnSO$_2$ relaxes back to the ground state *via* IC similar to AnSO$_2$Ph, but another portion ends up in a long-lived emissive state (>10 ns), which is likely the precursor for the photo-cycloaddition reaction. Unlike sulfur-bridged terthiophenes T$_3$SO$_n$, the main difference between AnS and AnSO$_2$ is the participation of the sulfur lone pair orbitals. Computational results suggest that the absence of lone pairs in the sulfone-bridge eliminates possible n(S) → σ* and n(S) → π* contributions to ISC and IC. The simplified relaxation dynamics are summarized in the Jablonski diagram in Fig. 13d. Increasing the oxidation state of the sulfur bridge can, in turn, tune the electronic structure of the linker atom which can modulate the relaxation pathways to enable divergent photochemistry.

Application of sulfoxide elimination photochemistry

Our group has leveraged the photochemical conversion of sulfoxide-bridged anthracene dimers, which are initially weakly emissive, to strongly emissive bianthracene photoproducts, as potential anti-counterfeiting materials for authentication technology. The dyes were used to formulate photoactive inks that can be used for patterning as the reaction is controlled spatially using light.[77] Inks were prepared by doping the dye into

a poly(N-vinylcarbazole) (PVK) host at 1 wt%. Additionally, we showed that luminescent patterns can be read using the camera of a smartphone illustrating the ease-of-use for this method, as it reduces the need for expensive and complex instruments required for validation.

The first demonstration by our group used AnSO-based inks to design multidimensional QR codes.[77] These 2D barcodes technically display 3D information, where barcodes provide two dimensions of positional information and a third dimension corresponding to an intensity of 0 or 1. Thus, by varying the intensity of a specific position from 0 to 1, the data density that can be encoded in a 2D barcode can be increased. Paper substrates were coated with the ink and exposed to 400 nm light through a shadow mask. The shadow mask used comprised of a 2D data matrix encoding the phrase "Hello World" layered on top of a variable transmittance pattern in the form of a radial gradient. After UV exposure, the printed image contained information regarding the data matrix while displaying a background which varies in intensity. The color intensity was extracted using a smartphone to demonstrate the capability of creating multidimensional barcodes.
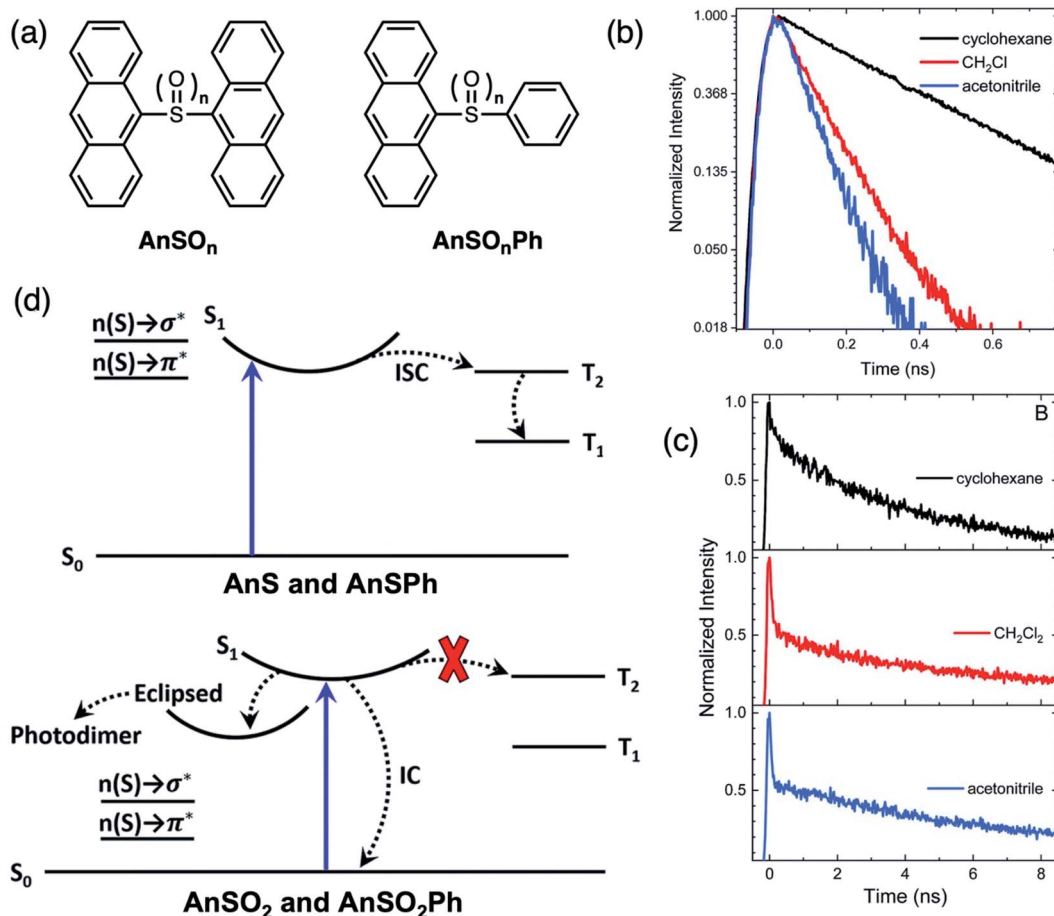
Fig. 13 (a) Structures of sulfur–bridged anthracene dimers **AnSO$_n$** and monomers **AnSO$_n$Ph** (n = 0, 2) reported by our group. (b) Normalized PL time traces on a natural log scale for **AnS** in cyclohexane (black), CH$_2$Cl$_2$ (red), and acetonitrile (blue) showing that PL lifetime decreases with increasing solvent polarity. (c) Normalized PL time traces integrated over all wavelengths for **AnSO$_2$** in cyclohexane (black), CH$_2$Cl$_2$ (red), acetonitrile (blue). (d) Simplified Jablonski diagram illustrating how mixing of the n(S) → σ* and n(S) → π* linker orbitals enable intersystem crossing (ISC) in the sulfide compounds, whereas the lack of mixing in the sulfone prevents ISC from occurring (red X). Adapted with permission from ref. 75. Copyright 2019 Royal Society of Chemistry.

The main disadvantage of covert luminescent patterns is their ease of reproducibility due to the vast number of dyes with similar emission characteristics (color) available. Thus stimuli-responsive inks, which respond to external factors such as light, have shown to be promising candidates for next-generation materials used in anti-counterfeiting applications. Following our first application of **AnSO**-based dyes, our group then designed and synthesized both a red and green emissive derivative that could be used in conjunction with **AnSO** (blue emissive) in order to achieve full color tuning.[78] Substitution at the 10,10′-position of the dianthracene core with triarylamine (**TAAAnSO**) and phenothiazine (**PTZAnSO**) groups afforded green and red emissive photoproducts, respectively, after irradiation (Fig. 14a). The unique optical properties of the individual sulfoxides allow for different rates of photoconversion, which can be initiated using specific irradiation wavelengths. This approach constitutes a new method for full color tuning since the final emission color of a mixture of the sulfoxides depends on (i) the mixing ratio, (ii) duration of light exposure and (iii) the irradiation wavelength. As a proof-of-concept, an inexpensive, publicly available smartphone application (app) called "Colorimeter" was used to determine the emission color of a mixture containing all three dyes after 1 minute of 400 nm light irradiation, and the corresponding CIELAB coordinates were extracted using the software (Fig. 14c). The final coordinates after light exposure of a specific duration can then be compared against a "true color" to determine the authenticity of a product. Additionally, the ability to visually monitor the "activation process" of this concept is novel to this system, as the mechanism of activation is based on the unique photochemistry of the sulfoxide-bridged dimers.

Sulfur-bridged ligands for Ir(III), Cu(I) and Ru(II) complexes

Drawing inspiration from the photophysical trends and emergence of novel photochemical pathways that were dependent on the oxidation state in symmetric sulfur-bridged π-conjugated materials, our group designed new diimine ligands for luminescent metal complexes (Fig. 15). The introduction of substituents such as electron-donating groups (EDGs) or
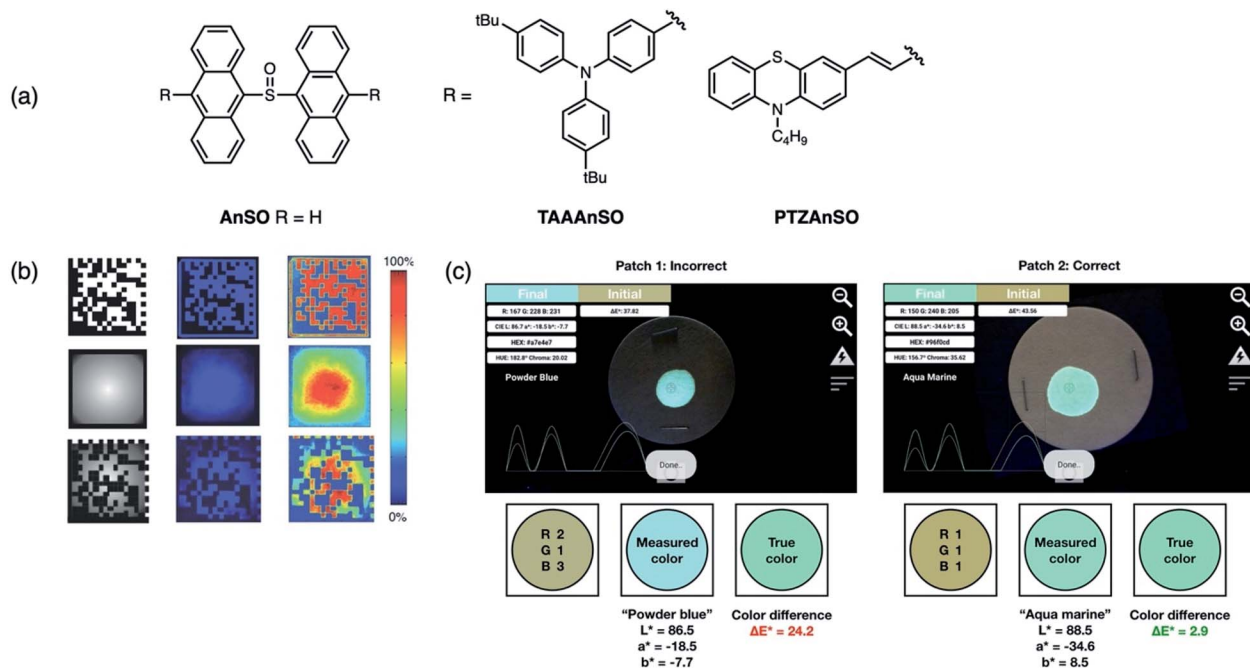
Fig. 14 (a) Structures of sulfoxide-bridged anthracene dimers **AnSO**, **TAAAnSO**, **PTZAnSO** reported by our group used to prepare inks for proof-of-concept demonstrations. (b) Using a two-stage mask that contains both a 2D data matrix and variable transmittance pattern (radial gradient to the center), a multidimensional fluorescent barcode can be patterned using UV light. The color intensity is measured using a smartphone camera. Adapted with permission from ref. 76. Copyright 2016 Wiley. (c) Software interface of *Colorimeter* used to extract CIELAB coordinates. These coordinates are compared to a "true color" to determine authenticity. Adapted with permission from ref. 77. Copyright 2019 Royal Society of Chemistry.

electron-withdrawing groups (EWGs) at, for example, the R^1 and/or R^2 position of 4,4'-bipyridine (bpy), can be used to modify the photophysical properties of the resulting metal complex. By incorporating a sulfur group in between the diimine groups, we introduced a second degree of tuning. The ability to systematically alter the sulfur centre provides a convenient approach for adjusting electron density on the ligand, which can then be used to fine tune the excited state electronics of luminescent metal complexes. The following section describes the use of sulfur-bridged dipyridyl (**DPS**) and dithiazolyl (**tzS**) ligands in Ir(III), Cu(I) and Ru(II) complexes, and how altering the oxidation state of the sulfur bridge on the ligand results in changes in the photophysical and/or electrochemical properties of the metal complex.

Since Ir(III) complexes are known for their high efficiency and wide scope of tunability in both OLEDs[79,80] and light-emitting electrochemical cells (LEECs),[81,82] sulfur-bridged dipyridyl ligands were first installed on Ir(III) metal centers (Fig. 16a).[83] Upon oxidizing the bridging sulfur atom from sulfide (**Ir-DPS**, **Ir-Me-DPS**) to sulfone (**Ir-DPSO$_2$**, **Ir-Me-DPSO$_2$**), the first reduction of the oxidized complex is shifted to a more positive potential (−1.26 and −1.73 V for **Ir-DPSO$_2$** and **Ir-Me-DPSO$_2$**, respectively) compared to the sulfide (−2.16 and −2.40 V for **Ir-DPS** and **Ir-Me-DPS**, respectively). This can be attributed to the electron-withdrawing nature of the sulfoxide and sulfone which leads to stabilization of the LUMO. The sulfide and sulfoxide (**Ir-DPSO**, **Ir-Me-DPSO**) complexes show almost identical fine-structured spectra with blue-green emission (Fig. 16b),

indicative of significant ligand-centered (^{3}LC) contributions to the lowest triplet excited state. This was further confirmed by solvatochromic behavior in the emission spectra and computational studies. **Ir-DPSO$_2$** and **Ir-Me-DPSO$_2$** on the other hand, exhibit pronounced metal-to-ligand and ligand-to-ligand charge transfer character (^{3}MLCT/^{3}LLCT) with broad and red-shifted emission bands. Complex **Ir-Me-DPSO$_2$**, with methyl substituents in the 4,4'-positions, shows a slight blue-shift (15 nm) compared to **Ir-DPSO$_2$**, which is consistent with previous reports.[84] PLQYs in deaerated CH_2Cl_2 were <0.01–0.08, slightly lower than that of the Ir(III) complex with bipyridine ligand (0.14) in deaerated CH_3CN, possibly due to increased flexibility of the ligand. Varying the oxidation state of the sulfur centre on these bridged dipyridyl ligands enables control over triplet excited state electronics and demonstrates "two-level" tuning over the emission color.

Emissive Cu(I) complexes have attracted great attention in the past decade due to the earth abundance of this metal and lower cost compared to Ir. Furthermore, the capability of Cu(I) complexes to undergo an additional radiative pathway *via* TADF significantly decreases the photoluminescent lifetime and enhances the quantum efficiency, which is beneficial for device efficiencies in OLEDs and LEECs.[85] In the ground-state, the Cu(I) center adopts a pseudotetrahedral geometry with a d^{10} configuration. Upon photoexcitation, the complex undergoes a fast (<1 ps) Jahn–Teller distortion to a more flattened d^9 geometry, opening up nonradiative decay pathways.[86–88] Therefore, rational design of the ligand by introducing steric
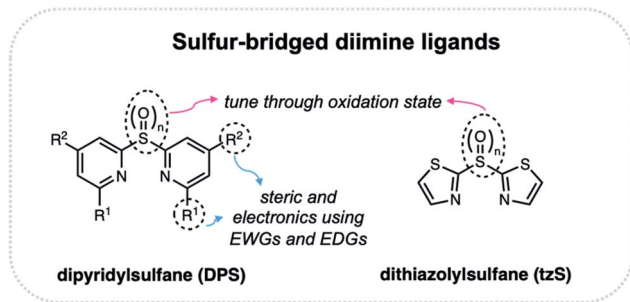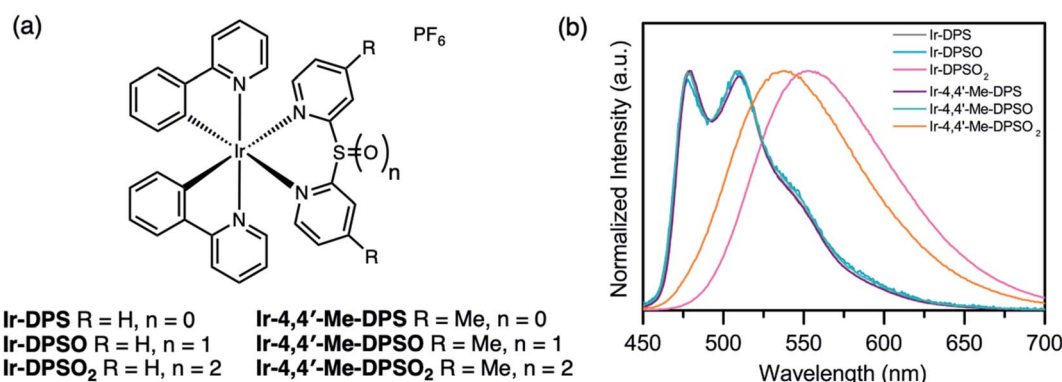
Fig. 15 Structure of 4,4′-bipyridine ligand (bpy) compared to sulfur-bridged diimine ligands based on dipyridylsulfane (**DPS**) and dithiazolylsulfane (**tzS**).

hindrance is crucial to inhibit this undesired distortion in order to maintain a tetrahedral geometry. Surprisingly, not only does sulfur oxidation alter excited state electronics, but it also provides a variety of interesting binding modes and complex geometries with changes in steric constraints (Fig. 17). Without any steric constraints, **Cu-DPS** and **Cu-DPSO₂** are mononuclear species with a distorted tetrahedral geometry at the Cu(I) center, retaining the typical N,N binding mode of the diimine ligand. However, with the introduction of methyl substituents on the 6- and 6′-position of the **DPS** ligand, complexes **Cu-Me-DPS** and **Cu-Me-DPSO₂** are bimetallic species with distorted trigonal geometries at the Cu(I) center, bridged by the bi[2-(diphenylphosphino)-phenyl] ether ligand (DPEphos). Upon sulfur oxidation, **Cu-Me-DPSO₂** was also found to exist as a bimetallic species, in this case with **Me-DPSO₂** as the bridging ligand through a N,O coordination mode. When the steric constraints are further increased to phenyl groups, monometallic species are formed again. **Cu-Ph-DPS** adopts a distorted trigonal geometry with the diimine ligand bound through only one pyridyl nitrogen. The sulfone group in **Cu-Ph-DPSO₂**

enables a N,O binding mode, forming a tetrahedral geometry at the Cu(I) metal center. All six complexes are weakly emissive in solution but more strongly emissive in the solid state with PLQYs up to 0.20. Interestingly, complexes **Cu-DPS**, **Cu-DPSO₂**, **Cu-Me-DPS**, **Cu-Me-DPSO₂** and **Cu-Ph-DPSO₂** all exhibit TADF while **Cu-Ph-DPS** shows triplet ligand-centered (^{3}LC) emission.

Interestingly, when sulfoxide-bridged diimine ligands are used, **Cu-DPSO** gives yellow-green luminescence with the same binding mode as **Cu-DPS** (Fig. 18a).[89] However, **Cu-Me-DPSO** with methyl substituents at the 6- and 6′-positions on the diimine ligand adopts a N,O binding mode in the single-crystal structure. It is also worth noting that in solution or bulk solid samples of **Cu-Me-DPSO**, only the typical N,N binding mode can be found, confirmed by NMR spectroscopy and powder X-ray diffraction. Surprisingly, unique phase-dependent and thermochromic emission was also observed (Fig. 18b and c). **Cu-Me-DPSO** was initially isolated as an amorphous powder (*a*-**Cu-Me-DPSO**), which is yellow emissive (542 nm) under a 365 nm UV hand lamp. Upon heating to 180 °C, a crystalline species (*c*-**Cu-Me-DPSO**) forms and emits orange fluorescence (658 nm). *c*-**Cu-Me-DPSO** also exhibits reversible thermochromic emission, whereby the complex undergoes a large emission color change from orange at room temperature (25 °C) to yellow (556 nm) at −196 °C (Fig. 18d). It is speculated that at room temperature, *c*-**Cu-Me-DPSO** adopts a more flattened geometry in the excited state, which gives rise to orange emission (Fig. 18e). However, at low temperatures or in the amorphous phase, the geometry of the excited state is closer to tetrahedral, leading to higher energy emission.[90–93] Emissive thermochromic Cu(I) complexes have been largely limited to Cu(I) halide clusters,[94,95] and this work provides a new avenue for the design of novel stimuli-responsive Cu(I) complexes.

More recently, sulfur-bridged bithiazole ligands were installed on both Cu(I) and Ru(II) complexes (Fig. 19a).[96] Both **Cu-tzS** and **Cu-tzSO$_n$** are weakly emissive in solution as radiative decay is often quenched in Cu(I) complexes by Jahn–Teller distortions, but exhibit strong emission as doped PMMA thin films since the degree of distortion is reduced when confined in a polymer matrix. The oxidation state of the sulfur-bridged

Fig. 16 (a) Structures of Ir(III) complexes **Ir-DPSO$_n$** and **Ir-Me-DPSO$_n$** (n = 0−2) reported by our group. (b) PL spectra of the Ir(III) complexes in CH₂Cl₂ solution (λ_{ex} = 390 nm). Adapted with permission from ref. 82. Copyright 2017 American Chemical Society.
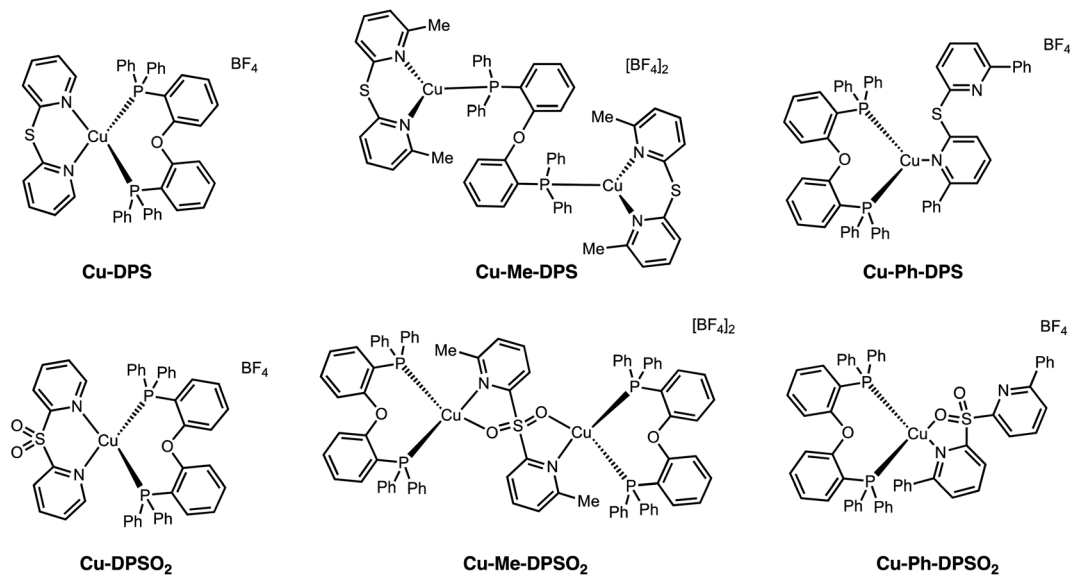
Fig. 17 Structures of Cu(I) complexes **Cu-DPSO$_n$**, **Cu-Me-DPSO$_n$** and **Cu-Ph-DPSO$_n$** (where $n = 0$ or 2) reported by our group.
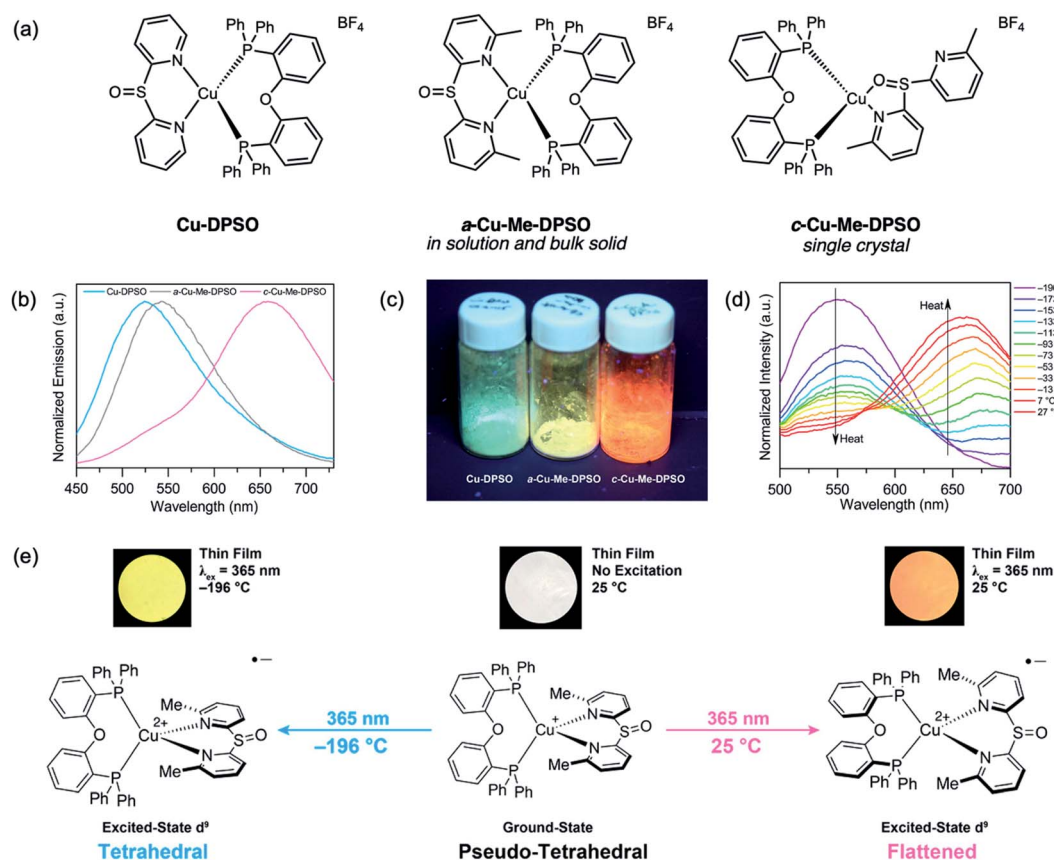
Fig. 18 (a) Structures of Cu(I) complexes **Cu-DPSO** and **Cu-Me-DPSO** reported by our group. (b) Room-temperature solid-state emission spectra of **Cu-DPSO**, *a*-**Cu-Me-DPSO** and *c*-**Cu-Me-DPSO** (drop-cast from MeOH, $\lambda_{ex} = 390$ nm). (c) Photographs of the Cu(I) complexes under UV excitation. (d) Variable-temperature solid-state emission spectra of *c*-**Cu-Me-DPSO** from −196 to 27 °C (drop-cast from MeOH, $\lambda_{ex} = 390$ nm). (e) Proposed excited-state conformational changes resulting in the thermochromic emission of *c*-**Cu-Me-DPSO**. Adapted with permission from ref. 88. Copyright 2018 American Chemical Society.

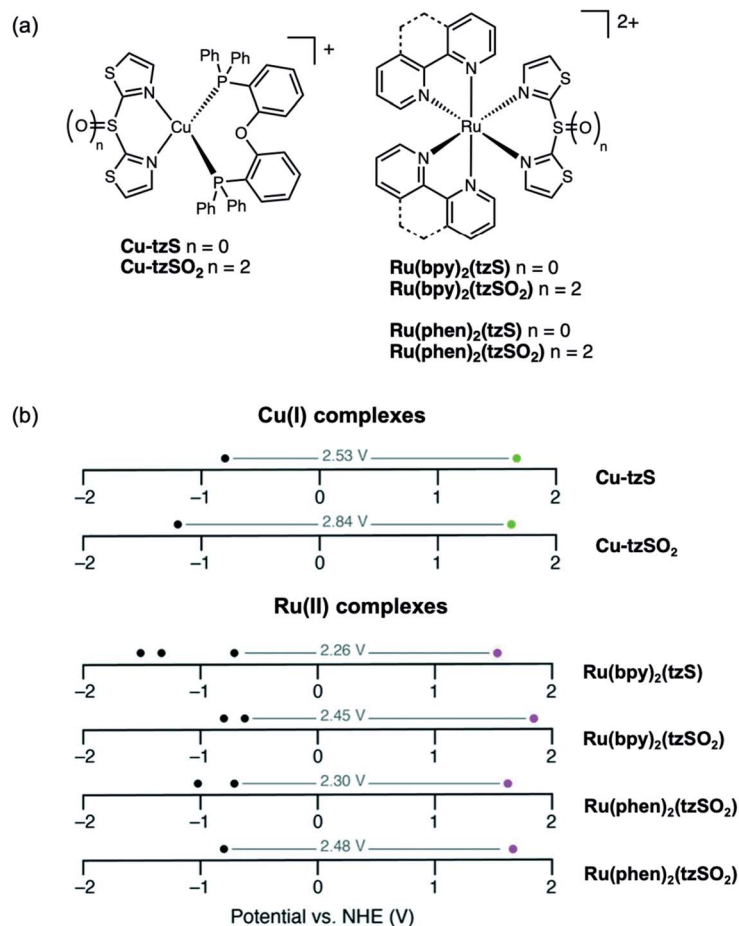Fig. 19 (a) Structures of **Cu-tzSO$_n$** and **Ru(bpy)$_2$(tzSO$_n$)** and **Ru(phen)$_2$(tzSO$_n$)** complexes reported by our group ($n = 0$, 2). (b) Redox potentials of Cu(I) and Ru(II) complexes with reductive (black dots) and oxidative (green or purple dots) potentials illustrated. Adapted with permission from ref. 95. Copyright 2019 Royal Society of Chemistry.

bithiazole ligand does not appear to influence the photo-physical properties of the Cu(I) complexes in this case. The Ru(II) complexes are non-emissive in solution and exhibit weak emission as both neat solid and doped PMMA thin films at room temperature (293 K). The emission intensity of the Ru(II) complexes as neat thin films and as frozen CH$_2$Cl$_2$ solutions increases when the samples were cooled to 77 K. On the other hand, the emission profiles at 77 K reveal that the nature of the **Ru(bpy)$_2$(tzSO$_n$)** emitting state depends on the oxidation state. **Ru(bpy)$_2$(tzS)** has structured emission, representative of a ^{3}MLCT emitting state compared to **Ru(bpy)$_2$(tzSO$_2$)** which displays a Gaussian-like emission band that is characteristic of a ^{3}MC emitting state. In these examples, the oxidation state of the ligand was shown to tune the electrochemical properties of both the Cu(I) and Ru(II) complexes (Fig. 19b). The redox potentials of complexes bearing sulfur-bridged ligands indicate smaller HOMO–LUMO gaps than for those with sulfone-bridged ligands. This suggests that altering the oxidation state of a bridging sulfur group on diimine ligands not only can influence photophysical properties but can be a useful handle for fine-tuning electrochemical properties of metal complexes as well.

Conclusions and outlook

Over the past decade, sulfur groups have been used to cova-lently link chromophores together to prepare symmetric dimers in π-conjugated materials. The identity of the chro-mophore can be altered to achieve distinct photophysical properties. Sulfur can serve as a passive linker, enabling through-space interactions between the subunits to induce electronic coupling. Perhaps the more intriguing aspect of sulfur as a bridging atom, is the accessibility of higher oxidation states. The lone pair electrons of sulfur can be used to form polarized bonds while maintaining nearly identical geometry. The ability to precisely control the electronic interactions from within the molecule without inducing large conformation changes, or without having to change the external environment (solvent polarity), make these scaffolds particularly interesting to study, and may also be useful for the design of functional materials.

The reports summarized have focussed on examining the CT contribution of excited state as a function of oxidation state. Careful selection of the chromophore in both small molecule and macromolecular systems furnished dimers that could

exhibit desirable properties such as enhanced PLQYs or room temperature phosphorescence (RTP). The screening effect of the lone pairs on the sulfur was shown to influence the amount of CT character in the singlet excited state. Oxidation to the sulfoxide and sulfone also resulted in a stabilizing effect on the CT state. This in turn affects ISC to the triplet state. Depending on whether it is desired to create or suppress these CT states, the efficiency of the radiative process from either the singlet or triplet state can thus be tuned. This concept of using oxidation states to modulate excited state dynamics in dimeric system can also promote photochemistry in anthracene-based systems, by enabling the formation of long-lived excited states that are presumed to be the precursors for photoproducts.

In addition to organic materials, sulfur bridges were used as a design strategy to prepare "two-level" tunable diimine ligands for luminescent metal complexes. Sulfur-bridged dipyridyl and dithiazoyl ligands were used to synthesize Ir(III), Cu(I) and Ru(II) complexes. In addition to peripheral functionalization of the dipyridyl ligand, oxidation of the sulfur bridge could also result in various complex geometries with the oxygen as the coordinating atom. Oxidation of the bridging sulfur can alter the emission properties such as color and lifetime, as well as give rise to new photophysical phenomena such as thermally activated delayed fluorescence (TADF) or thermochromism.

Beyond the examples presented in this perspective, it is anticipated that other processes that require precise control of chromophore–chromophore interactions should benefit from this design strategy such as photon upconversion[97] or intramolecular singlet fission.[98] For example, the extent of coupling between chromophores plays a critical role in intramolecular singlet fission in bridged chromophore dimers. The introduction of a sulfur bridge and subsequent oxidation in these systems should allow for modulation of processes including exciton formation and recombination. On the other hand, oxidation of a bridging sulfur in ligands is useful beyond altering the emission characteristics of luminescent metal complexes. These ligands can also be used to control electronic communication between two metal complexes,[99] and in turn, effect electron transfer rates, which is crucial for developing systems capable of artificial photosynthesis[100] or photocatalytic reactions.[101] Likewise, the use of a sulfur bridge can covalently tether the photosensitizer (PS) and catalyst together, and oxidation can potentially optimize these light-stimulated processes. Incorporating sulfur bridges as a molecular design strategy will benefit the discovery of novel organosulfur compounds by offering an opportunity to fine tune optical, electronic and redox properties through systematic oxidation.

Author contributions

J. Y. and Z. X. contributed equally to the writing of this manuscript with input and direction from M. O. W.

Conflicts of interest

The authors have no conflicts to declare.

Acknowledgements

References

1 G. D. Considine, in *Van Nostrand's Scientific Encyclopedia*, John Wiley & Sons, Inc., Hoboken, NJ, USA, 2005.

2 R. Hell, M. S. Khan and M. Wirtz, in *Plant Cell Monographs*, ed. R. Hell and R.-R. Mendel, Springer Berlin Heidelberg, Berlin, Heidelberg, 2010, vol. 17, pp. 243–279.

3 K. A. Scott and J. T. Njardarson, *Top. Curr. Chem.*, 2018, **376**, 5.

4 R. Cecil and J. R. Mcphee, in *Advances in Protein Chemistry*, ed. C. B. Anfinsen Jr, M. L. Anson, K. Bailey and J. T. Edsall, Academic Press, New York and London, 1959, vol. 14, pp. 255–389.

5 S. F. Betz, *Protein Sci.*, 1993, **2**, 1551–1558.

6 E. A. Ilardi, E. Vitaku and J. T. Njardarson, *J. Med. Chem.*, 2014, **57**, 2832–2842.

7 P. Devendar and G.-F. Yang, in *Sulfur Chemistry. Topics in Current Chemistry Collections*, ed. X. Jiang, Springer International Publishing, Cham, 2019, pp. 35–78.

8 C. Lamberth, *J. Sulfur Chem.*, 2004, **25**, 39–62.

9 H. Mutlu, E. B. Ceper, X. Li, J. Yang, W. Dong, M. M. Ozmen and P. Theato, *Macromol. Rapid Commun.*, 2019, **40**, 1800650.

10 Y. Li, J.-Y. Liu, Y.-D. Zhao and Y.-C. Cao, *Mater. Today*, 2017, **20**, 258–266.

11 S. C. Rasmussen, S. J. Evenson and C. B. McCausland, *Chem. Commun.*, 2015, **51**, 4528–4543.

12 T. Baumgartner, *J. Inorg. Organomet. Polym. Mater.*, 2005, **15**, 389–409.

13 C. Wang, H. Dong, W. Hu, Y. Liu and D. Zhu, *Chem. Rev.*, 2012, **112**, 2208–2267.

14 J. E. Anthony, *Chem. Rev.*, 2006, **106**, 5028–5048.

15 A. R. Murphy and J. M. J. Fréchet, *Chem. Rev.*, 2007, **107**, 1066–1096.

16 K. Takimiya, S. Shinamura, I. Osaka and E. Miyazaki, *Adv. Mater.*, 2011, **23**, 4347–4370.

17 G. Barbarella, M. Melucci and G. Sotgiu, *Adv. Mater.*, 2005, **17**, 1581–1593.

18 T. P. Kaloni, P. K. Giesbrecht, G. Schreckenbach and M. S. Freund, *Chem. Mater.*, 2017, **29**, 10248–10283.

19 K. Tanaka, S. Wang and T. Yamabe, *Synth. Met.*, 1989, **30**, 57–65.

20 G. Barbarella, L. Favaretto, G. Sotgiu, M. Zambianchi, L. Antolini, O. Pudova and A. Bongini, *J. Org. Chem.*, 1998, **63**, 5497–5506.

21 G. Barbarella, O. Pudova, C. Arbizzani, M. Mastragostino and A. Bongini, *J. Org. Chem.*, 1998, **63**, 1742–1745.

22 G. Barbarella, L. Favaretto, G. Sotgiu, M. Zambianchi, V. Fattori, M. Cocchi, F. Cacialli, G. Gigli and R. Cingolani, *Adv. Mater.*, 1999, **11**, 1375–1379.

23 Y. Suzuki, T. Okamoto, A. Wakamiya and S. Yamaguchi, *Org. Lett.*, 2008, **10**, 3393–3396.

24 B. Chen, H. Zhang, W. Luo, H. Nie, R. Hu, A. Qin, Z. Zhao and B. Z. Tang, *J. Mater. Chem. C*, 2017, **5**, 960–968.

25 Q. Yang, D. Li, W. Chi, R. Guo, B. Yan, J. Lan, X. Liu and J. Yin, *J. Mater. Chem. C*, 2019, **7**, 8244–8249.

26 C. P. Hsu, *Acc. Chem. Res.*, 2009, **42**, 509–518.

27 J. C. Johnson, A. J. Nozik and J. Michl, *Acc. Chem. Res.*, 2013, **46**, 1290–1299.

28 D. A. da Silva Filho, E.-G. Kim and J.-L. Brédas, *Adv. Mater.*, 2005, **17**, 1072–1076.

29 J. Ahrens, B. Böker, K. Brandhorst, M. Funk and M. Bröring, *Chem. - Eur J.*, 2013, **19**, 11382–11395.

30 T. Eder, T. Stangl, M. Gmelch, K. Remmerssen, D. Laux, S. Höger, J. M. Lupton and J. Vogelsang, *Nat. Commun.*, 2017, **8**, 1641.

31 K. Kilså, J. Kajanus, J. Mårtensson and B. Albinsson, *J. Phys. Chem. B*, 1999, **103**, 7329–7339.

32 A. Satake and Y. Kobuke, *Org. Biomol. Chem.*, 2007, **5**, 1679–1691.

33 Y. Sasano, R. Sato, Y. Shigeta, N. Yasuda and H. Maeda, *J. Org. Chem.*, 2017, **82**, 11166–11172.

34 A. A. Ryan, S. Plunkett, A. Casey, T. McCabe and M. O. Senge, *Chem. Commun.*, 2014, **50**, 353–355.

35 G. Copley, D. Shimizu, J. Oh, J. Sung, K. Furukawa, D. Kim and A. Osuka, *Eur. J. Org. Chem.*, 2016, **2016**, 1977–1981.

36 F. B. Dias, K. N. Bourdakos, V. Jankus, K. C. Moss, K. T. Kamtekar, V. Bhalla, J. Santos, M. R. Bryce and A. P. Monkman, *Adv. Mater.*, 2013, **25**, 3707–3714.

37 Z. Yang, Z. Mao, Z. Xie, Y. Zhang, S. Liu, J. Zhao, J. Xu, Z. Chi and M. P. Aldred, *Chem. Soc. Rev.*, 2017, **46**, 915–1016.

38 Q. Zhang, J. Li, K. Shizu, S. Huang, S. Hirata, H. Miyazaki and C. Adachi, *J. Am. Chem. Soc.*, 2012, **134**, 14706–14709.

39 S. Wu, M. Aonuma, Q. Zhang, S. Huang, T. Nakagawa, K. Kuwabara and C. Adachi, *J. Mater. Chem. C*, 2014, **2**, 421–424.

40 Q. Zhang, B. Li, S. Huang, H. Nomura, H. Tanaka and C. Adachi, *Nat. Photonics*, 2014, **8**, 326–332.

41 Q. Zhang, D. Tsang, H. Kuwabara, Y. Hatae, B. Li, T. Takahashi, S. Y. Lee, T. Yasuda and C. Adachi, *Adv. Mater.*, 2015, **27**, 2096–2100.

42 G. H. Lee and Y. S. Kim, *Polym. Bull.*, 2016, **73**, 2439–2446.

43 S. Xu, T. Liu, Y. Mu, Y.-F. Wang, Z. Chi, C.-C. Lo, S. Liu, Y. Zhang, A. Lien and J. Xu, *Angew. Chem. Int. Ed.*, 2015, **54**, 874–878.

44 M. Monçalves, D. S. Rampon, P. H. Schneider, F. S. Rodembusch and C. C. Silveira, *Dyes Pigments*, 2014, **102**, 71–78.

45 M. Monçalves, G. M. Zanotto, J. M. Toldo, D. S. Rampon, P. H. Schneider, P. F. B. Gonçalves, F. S. Rodembusch and C. C. Silveira, *RSC Adv.*, 2017, **7**, 8832–8842.

46 P. R. Christensen, J. K. Nagle, A. Bhatti and M. O. Wolf, *J. Am. Chem. Soc.*, 2013, **135**, 8109–8112.

47 C. D. Cruz, P. R. Christensen, E. L. Chronister, D. Casanova, M. O. Wolf and C. J. Bardeen, *J. Am. Chem. Soc.*, 2015, **137**, 12552–12564.

48 C. Climent, M. Barbatti, M. O. Wolf, C. J. Bardeen and D. Casanova, *Chem. Sci.*, 2017, **8**, 4941–4950.

49 R. S. Kathayat, L. Yang, T. Sattasathuchana, L. Zoppi, K. K. Baldridge, A. Linden and N. S. Finney, *J. Am. Chem. Soc.*, 2016, **138**, 15889–15895.

50 E. Caron and M. O. Wolf, *Macromolecules*, 2017, **50**, 7543–7549.

51 M. H. M. Cativo, A. C. Kamps, J. Gao, J. K. Grey, G. R. Hutchison and S. J. Park, *J. Phys. Chem. B*, 2013, **117**, 4528–4535.

52 S. Wei, J. Xia, E. J. Dell, Y. Jiang, R. Song, H. Lee, P. Rodenbough, A. L. Briseno and L. M. Campos, *Angew. Chem. Int. Ed.*, 2014, **53**, 1832–1836.

53 E. L. Dane, S. B. King and T. M. Swager, *J. Am. Chem. Soc.*, 2010, **132**, 7758–7768.

54 Z. Zhou, W. Huang, Y. Long, Y. Chen, Q. Yu, Y. Zhang, S. Liu, Z. Chi, X. Chen and J. Xu, *J. Mater. Chem. C*, 2017, **5**, 8545–8552.

55 A. Forni, E. Lucenti, C. Botta and E. Cariati, *J. Mater. Chem. C*, 2018, **6**, 4603–4626.

56 Kenry, C. Chen and B. Liu, *Nat. Commun.*, 2019, **10**, 2111.

57 Q. Li, Y. Tang, W. Hu and Z. Li, *Small*, 2018, **14**, 1801560.

58 S. K. Lower and M. A. El-Sayed, *Chem. Rev.*, 1966, **66**, 199–241.

59 H. Ma, Q. Peng, Z. An, W. Huang and Z. Shuai, *J. Am. Chem. Soc.*, 2019, **141**, 1010–1015.

60 Z. Xu, C. Climent, C. M. Brown, D. Hean, C. J. Bardeen, D. Casanova and M. O. Wolf, *Chem. Sci.*, 2021, **12**, 188–195.

61 Z. Yang, Z. Mao, X. Zhang, D. Ou, Y. Mu, Y. Zhang, C. Zhao, S. Liu, Z. Chi, J. Xu, Y.-C. Wu, P.-Y. Lu, A. Lien and M. R. Bryce, *Angew. Chem. Int. Ed.*, 2016, **55**, 2181–2185.

62 Y. Hu, Z. Wang, X. Jiang, X. Cai, S.-J. Su, F. Huang and Y. Cao, *Chem. Commun.*, 2018, **54**, 7850–7853.

63 L. Zhan, Z. Chen, S. Gong, Y. Xiang, F. Ni, X. Zeng, G. Xie and C. Yang, *Angew. Chem. Int. Ed.*, 2019, **58**, 17651–17655.

64 Z. Mao, Z. Yang, Z. Fan, E. Ubba, W. Li, Y. Li, J. Zhao, Z. Yang, M. P. Aldred and Z. Chi, *Chem. Sci.*, 2019, **10**, 179–184.

65 P. R. Christensen, B. O. Patrick, É. Caron and M. O. Wolf, *Angew. Chem. Int. Ed.*, 2013, **52**, 12946–12950.

66 R. S. Grainger, B. Patel, B. M. Kariuki, L. Male and N. Spencer, *J. Am. Chem. Soc.*, 2011, **133**, 5843–5852.

67 S. Hayakawa, K. Matsuo, H. Yamada, N. Fukui and H. Shinokubo, *J. Am. Chem. Soc.*, 2020, **142**, 11663–11668.

68 G. E. Hartzell and J. N. Paige, *J. Am. Chem. Soc.*, 1966, **88**, 2616–2617.

69 R. M. Dodson and R. F. Sauers, *Chem. Commun.*, 1967, 1189–1190.

70 I. A. Abu-Yousef and D. N. Harpp, *Tetrahedron Lett.*, 1995, **36**, 201–204.

71 I. A. Abu-Yousef and D. N. Harpp, *J. Org. Chem.*, 1997, **62**, 8366–8371.

72 L. E. Longobardi, V. Wolter and D. W. Stephan, *Angew. Chem. Int. Ed.*, 2015, **54**, 809–812.

73 M. Joost, M. Nava, W. J. Transue, M. A. Martin-Drumel, M. C. McCarthy, D. Patterson and C. C. Cummins, *Proc. Natl. Acad. Sci. U. S. A.*, 2018, **115**, 5866–5871.

74 H. Bouas-Laurent, A. Castellan, J. P. Desvergne and R. Lapouyade, *Chem. Soc. Rev.*, 2001, **30**, 248–263.

75 H. Bouas-Laurent, J.-P. Desvergne, A. Castellan and R. Lapouyade, *Chem. Soc. Rev.*, 2001, **30**, 248–263.

76 C. D. Cruz, J. Yuan, C. Climent, N. T. Tierce, P. R. Christensen, E. L. Chronister, D. Casanova, M. O. Wolf and C. J. Bardeen, *Chem. Sci.*, 2019, **10**, 7561–7573.

77 P. R. Christensen and M. O. Wolf, *Adv. Funct. Mater.*, 2016, **26**, 8471–8477.

78 J. Yuan, P. R. Christensen and M. O. Wolf, *Chem. Sci.*, 2019, **10**, 10113–10121.

79 T.-Y. Li, J. Wu, Z.-G. Wu, Y.-X. Zheng, J.-L. Zuo and Y. Pan, *Coord. Chem. Rev.*, 2018, **374**, 55–92.

80 G. Zhou, W. Y. Wong and X. Yang, *Chem. Asian J.*, 2011, **6**, 1706–1727.

81 T. Hu, L. He, L. Duan and Y. Qiu, *J. Mater. Chem.*, 2012, **22**, 4206–4215.

82 C. E. Housecroft and E. C. Constable, *Coord. Chem. Rev.*, 2017, **350**, 155–177.

83 C. M. Brown, M. J. Kitt, Z. Xu, D. Hean, M. B. Ezhova and M. O. Wolf, *Inorg. Chem.*, 2017, **56**, 15110–15118.

84 R. D. Costa, E. Ortí, D. Tordera, A. Pertegás, H. J. Bolink, S. Graber, C. E. Housecroft, L. Sachno, M. Neuburger and E. C. Constable, *Adv. Energy Mater.*, 2011, **1**, 282–290.

85 C. M. Brown, C. Li, V. Carta, W. Li, Z. Xu, P. H. F. Stroppa, I. D. W. Samuel, E. Zysman-Colman and M. O. Wolf, *Inorg. Chem.*, 2019, **58**, 7156–7168.

86 Z. A. Siddique, Y. Yamamoto, T. Ohno and K. Nozaki, *Inorg. Chem.*, 2003, **42**, 6366–6378.

87 S. Garakyaraghi, E. O. Danilov, C. E. McCusker and F. N. Castellano, *J. Phys. Chem. A*, 2015, **119**, 3181–3193.

88 A. O. Razgoniaev, C. E. McCusker, F. N. Castellano and A. D. Ostrowski, *ACS Macro Lett.*, 2017, **6**, 920–924.

89 C. M. Brown, V. Carta and M. O. Wolf, *Chem. Mater.*, 2018, **30**, 5786–5795.

90 M. Iwamura, S. Takeuchi and T. Tahara, *J. Am. Chem. Soc.*, 2007, **129**, 5248–5256.

91 A. B. P. Lever, E. Mantovani and J. C. Donini, *Inorg. Chem.*, 1971, **10**, 2424–2427.

92 A. B. P. Lever and E. Mantovani, *Inorg. Chem.*, 1971, **10**, 817–826.

93 I. Grenthe, P. Paoletti, M. Sandstrom and S. Glikberg, *Inorg. Chem.*, 1979, **18**, 2687–2692.

94 S. Perruchas, X. F. Le Goff, S. Maron, I. Maurin, F. Guillen, A. Garcia, T. Gacoin and J.-P. Boilot, *J. Am. Chem. Soc.*, 2010, **132**, 10967–10969.

95 B. Huitorel, Q. Benito, A. Fargues, A. Garcia, T. Gacoin, J.-P. Boilot, S. Perruchas and F. Camerel, *Chem. Mater.*, 2016, **28**, 8190–8200.

96 E. Caron, C. M. Brown, D. Hean and M. O. Wolf, *Dalton Trans.*, 2019, **48**, 1263–1274.

97 A. B. Pun, S. N. Sanders, M. Y. Sfeir, L. M. Campos and D. N. Congreve, *Chem. Sci.*, 2019, **10**, 3969–3975.

98 C. Hetzer, D. M. Guldi and R. R. Tykwinski, *Chem. - Eur J.*, 2018, **24**, 8245–8257.

99 C. M. Brown, T. Auvray, E. E. Deluca, M. B. Ezhova, G. S. Hanan and M. O. Wolf, *Chem. Commun.*, 2020, **56**, 10750–10753.

100 M. D. Kärkäs, E. V Johnston, O. Verho and B. Åkermark, *Acc. Chem. Res.*, 2014, **47**, 100–111.

101 Y. Yamazaki, H. Takeda and O. Ishitani, *J. Photochem. Photobiol., C*, 2015, **25**, 106–137.